

Thermo-acoustic Engine Pressure Wave: Analysis of Working Fluid Effect

Somayya Esmat Elshabrawy, Mohammed Noorul Hussain, Isam Janajreh*

Mechanical Engineering Department, Khalifa University of Science and Technology, Masdar Institute, PO Box 54224, Abu Dhabi, United Arab Emirates

Received 3 October, 2019

Abstract

Thermo-acoustic Engines (TAE) utilize the production of acoustic waves to generate mechanical power when a thermal gradient is applied to a stack placed in the resonator of TAE. Owing to non-existence of moving parts that a conventional engine has, TAEs are typically mechanically more efficient and reliable, hence are an important area of research. The thermo-acoustic phenomenon for TAEs is only driven by temperature gradient that induces fluid flow. However, in the previous works related to numerical study of standing wave TAEs, an initial disturbance in the form of pressure gradient has been imposed to generate fluid flow. In this paper, a 2D numerical analysis of a standing wave TAE is performed using computational fluid dynamics (CFD) modeling to capture the pressure fluctuations (without any initial disturbance) with time in the resonator channel in order to assess its thermo-acoustic performance. The results are obtained for pressure variation at specific points and the development of temperature profiles within the resonator. Using the pressure variations, FFT analysis was performed to identify sound pressure levels and resonant frequencies. Also, a sensitivity study has been carried out. The objective is to analyze the pressure wave development under different fluid properties. In this study, equivalent properties of a certain mixture of gases are prescribed to represent a composite working fluid. Two cases are considered i.e. mixture of air and helium and mixture of air and carbon dioxide. The compositions are varied in each case. It is noticed that in He mixtures the onset of pressure wave is quicker than in only air or CO₂ mixtures, this due to the higher thermal conductivities. However, when only He is considered there is no pressure wave unlike only air or only CO₂ cases due to low molecular weight. Frequency in He mixtures rises as He composition is increased, and the contrary is seen in CO₂ mixtures. This is due to the collective consequence of the Cp, thermal conductivity and molecular weight. The study shows how important the thermal properties of the working fluid are for the pressure wave.

© 2019 Jordan Journal of Mechanical and Industrial Engineering. All rights reserved

Keywords: Thermo-acoustic engine, Stirling cycle, refrigeration;

Nonmenclature

Abbreviations

TAE	Thermo-acoustic Engines
COP	Coefficient of Performance
CFD	Computational Fluid Dynamics
CFL	Friedrichs Lewy number

Symbols

ρ	Density
μ	Dynamic viscosity
ν	Kinematic viscosity
δ_x	Thermal penetration length
δ_v	Viscous penetration length
c_p	Specific Heat
ω	Angular frequency
κ	Thermal diffusivity
k	Thermal conductivity

1.

Introduction

Thermo-acoustic heat engines (TAE) are devices that convert thermal energy to acoustic energy with the advantage of the absence of moving parts [1] and using the Stirling engine cycle principle. This gives them the potential to be more reliable, low cost as they can operate without exotic materials and precision machining or tight tolerance. Decays of developments have pushed the efficiency of today's Internal combustion engines to 30% and as high as 40% for large diesel engine. The Coefficient of Performance (COP) of the vapor-compression refrigeration systems can also reach 50% of Carnot's COP. Although the potential exists for thermo-acoustic engine, these efficiencies are still unattained and pose some technical challenges.

In the Stirling cycle, a working gas is compressed in a piston cylinder arrangement, while a heat sink is actively absorbing the excess heat to keep the temperature of the gas constant. T_{gas} is then flowing through a

* Corresponding author e-mail: isam.janajreh@ku.ac.ae

regenerator/stack where it absorbs heat at constant volume. It is further heated at the heat source where it expands to deliver power to a piston [2]. Researchers like Ceperley[3] worked on replacing the pistons in a Stirling engine with sound waves and created the very first thermo-acoustic heat engine technology. As the Stirling engine experiences similar pressure-velocity dephasing as those occurs in a travelling acoustic wave, the development of standing wave thermo-acoustic engines and refrigerators are evolved by Los Alamos group. These are the two types of the thermo-acoustic engines, the moving/travelling -wave and the standing wave. In both systems the main component is the regenerator or stack, which is a porous solid medium that consists of heating plates, placed between two heat exchangers to transfer heat to/from the external thermal reservoirs and the working fluid.

Moreover, the thermal (δ_κ) and viscous (δ_ν) penetration depths are indicative of the boundary effect beyond which unnoticeable diffusion of heat or momentum can be felt within the oscillating period. This puts a limit to stack spacing and is defined as:

$$\delta_\kappa = \sqrt{2\kappa/\omega}, \text{ where } \kappa = k/\rho c_p \quad (1)$$

$$\delta_\nu = \sqrt{2\nu/\omega}, \text{ where } \nu = \mu/\rho \quad (2)$$

Where κ is the thermal diffusivity and k is the thermal conductivity of the working gas, ρ is the density, μ and ν are the dynamic and kinematic viscosities and c_p is the specific heat. Successful operation of a standing wave engine requires deliberately imperfect thermal contact between the gas and the stack, which is obtained when the spacing between the plates is roughly a few δ_κ . The ratio of $\delta_\kappa/\delta_\nu = \pi c_p/k$ is identified as the square root of Prandtl number, which is near unity for common gases and vindicating an equal order of thermal and viscous penetration. It is worth noting that in thermo-acoustic engine these penetration lengths are at much smaller length than the displacement amplitude, which is smaller than the acoustic wave length.

In literature thermoacoustic engines have been investigated and designed both experimentally and with computational fluid dynamics. Nijeholt et al[5] simulated a travelling wave thermoacoustic engine via a 2D CFD model. The authors reported that effects like streaming mass flows and vortices formation can be visualized, which was otherwise impossible when linear theory is used. Designs of thermoacoustic engines with looped tubes has been presented by Yazaki et al[6]. The design was built and tested experimentally. Results showed that looped tubes acted as wave power amplifiers and the onset temperature ratios were smaller in the loop. Biwa et al [7] experimentally investigated the lowest critical temperature ratio necessary to run a thermoacousticstirling engine. They showed a 32% decrease in critical temperature ratio by using up to 5 differentially heated generators. Other works have shown the application of thermoacoustic engines as electric generators and refrigerators[8][9].

In previous work by the authors [4] physical parameters like effect of length and temperature gradient have been studied. In this work, the focus is on the fluid dynamic aspect that is characteristic to the working fluid since it is not well investigated. Mixture of air with

helium and air with carbon dioxide are studied as cases, where the equivalent viscosity, thermal conductivity and specific heat with varying compositions are represent new working fluids.

2. Methodology

An axisymmetric cylindrical TAE is modeled in Ansys Fluent. The geometry is similar to that in the previous work by the authors [4] and is shown in Fig. 1. It shows the asymmetrical geometry of the discretized model mesh representing a stack of horizontal plates modeled at plate thickness of 5mm and a gap of 5 mm between each plate.

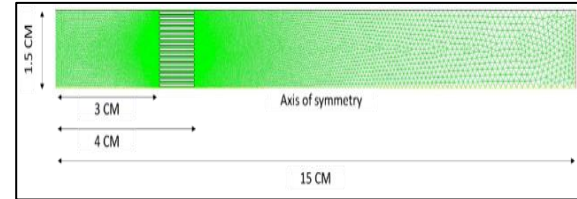


Figure 1. Modeled TAE baseline geometry in Fluent

The numerical model is based on the transient, non-isothermal and 2D cylindrical Navier-Stokes flow. The ideal gas model is assumed to govern the fluid state, as the developed pressure wave is relatively small. Turbulence is accounted for following the averaging of these equations where the resulted Reynolds stresses are modeled via the common eddy viscosity ($-\rho V_i V_j' = \mu_t (\partial V_i / \partial V_j + \partial V_j / \partial V_i)$) and k- ϵ transport model. Eq. 3-8 describe the overall governing equations (Eq. 3 the continuity, Eqs. 4, 5, and 6 the momentums, Eq. 8 is the general transport equation for any of the scalar quantity like those that govern the turbulence-k and - ϵ following the common eddy viscosity model. Eq. 9 governs the energy equation).

The continuity equation is as follows for axisymmetric geometries:

$$\frac{\partial \rho}{\partial t} + \frac{\partial(\rho V_x)}{\partial x} + \frac{\partial(\rho V_r)}{\partial r} + \frac{\rho V_r}{r} = 0 \quad (3)$$

Where x is the axial coordinate, r is the radial coordinate, V_x is the axial velocity, and V_r is the radial velocity. The momentum equation is written as:

$$\frac{\partial(\rho \vec{V})}{\partial t} + \nabla \cdot (\rho \vec{V} \vec{V}) = -\nabla p + \nabla \cdot \mu [(\nabla \vec{V} + \nabla \vec{V}^T) - \frac{2}{3} \nabla \cdot \vec{V} I] + \rho \vec{g} \quad (4)$$

Where ρ is the static pressure, μ is the molecular viscosity, and I is the unit tensor and its term accounts to the effect of volume dilation/expansion. The $\rho \vec{g}$ term is the gravitational body forces vector. In 2D axisymmetric geometries the axial and radial conservation of momentum equations are written as:

$$\frac{\partial \rho V_x}{\partial t} + \frac{1}{r} \frac{\partial}{\partial x} (r \rho V_x V_x) + \frac{1}{r} \frac{\partial}{\partial r} (r \rho V_r V_x) = -\frac{\partial p}{\partial x} + \frac{1}{r} \frac{\partial}{\partial x} [r \mu (2 \frac{\partial V_x}{\partial x} - \frac{2}{3} (\nabla \cdot \vec{V}))] + \frac{1}{r} \frac{\partial}{\partial r} [r \mu (\frac{\partial V_x}{\partial r} - \frac{\partial V_r}{\partial x})] + \rho g_x \quad (5)$$

$$\frac{\partial \rho V_r}{\partial t} + \frac{1}{r} \frac{\partial}{\partial x} (r \rho V_x V_r) + \frac{1}{r} \frac{\partial}{\partial r} (r \rho V_r V_r) = - \frac{\partial p}{\partial r} + \frac{1}{r} \frac{\partial}{\partial x} \left[r \mu \left(\frac{\partial V_r}{\partial x} + \frac{\partial V_x}{\partial r} \right) \right] + \frac{1}{r} \frac{\partial}{\partial r} \left[r \mu \left(2 \frac{\partial V_r}{\partial r} - \frac{2}{3} (\nabla \cdot \vec{V}) \right) \right] - 2 \mu \frac{V_r}{r^2} + \frac{2 \mu}{3 r} (\nabla \cdot \vec{V}) + \rho g_r \tag{6}$$

Divergence in axisymmetric geometrics is as:

$$\nabla \cdot \vec{V} = \frac{\partial V_x}{\partial x} + \frac{\partial V_r}{\partial r} + \frac{V_r}{r} \tag{7}$$

The transport equation in terms of ϕ dependent variable and in particular for each of the two turbulence scalars is written following the common four term formulation, i.e. temporal, advective, diffusive and any additional sources as:

$$\frac{\partial(\rho \phi)}{\partial t} + \nabla \cdot (\rho \vec{V} \phi - \Gamma \nabla \phi) = S_{\phi_k} \tag{8}$$

Where ϕ corresponds once to turbulent kinetic energy (k) and second to its dissipation rate (ϵ); Γ is the diffusion coefficient and S is the source term corresponding to each of the scalar equations. The k and ϵ equations are related by the eddy viscosity term such that $\mu_T = C_{\epsilon 2} \rho \frac{\epsilon^2}{k}$ where μ_T the turbulent viscosity. The internal energy (E) equation is written as:

$$\frac{\partial(\rho E)}{\partial t} + \nabla \cdot (\rho \vec{V} (\rho E + p)) = - \nabla \cdot [K \nabla T + (\mu (\nabla \vec{V} + \nabla \vec{V}^T) - \frac{2}{3} \nabla \cdot \vec{V} I) \cdot \vec{V}] \tag{9}$$

Where ρ is the density, V represents the velocity field, p is the flow pressure, μ is the dynamic viscosity, μ_T is the turbulent viscosity. The internal system energy (E) can be described as:

$$E = H - p/\rho + \frac{1}{2} \vec{V} \cdot \vec{V} \tag{10}$$

Where H is the system enthalpy, which related to internal energy by the static pressure and density term per Eq. 10. Equations 3-10 are solved numerically in computing the physical quantities. First the geometry or the computation domain is discretized. Then, these differential equations are integrated over the finite volume of a computational cell and over a finite time where a second-order central difference scheme is used in the discretization of the convective and diffusive terms while first-order fully implicit scheme used for time.

With respect to boundary conditions, all walls except the outlet are prescribed no slip. A free pressure outflow is prescribed at the outlet. The temperature at the stack walls is crucial, for the horizontal walls of each stack a decreasing temperature gradient profile is prescribed from 1000K to 300 K. The vertical walls of the stack are prescribed a $50 \text{ Wm}^{-2}\text{K}^{-1}$ heat transfer coefficient. The model is initially computed with a steady state, with a prescribed pressure (10 Pa. [4]) at the left closed wall, to create a minute velocity in the system, as is the practical case. Further on transient computation follows with a time step of 1E-5s, in accordance with the Courant Friedrichs Lewy number (CFL) principal. The pressure wave development, frequency and amplitude are analyzed.

3. Results and Discussion

3.1. Mesh sensitivity

In line with the authors' previous work, four levels of mesh were used to assess the solution independence, i.e. fine, baseline, and coarse-1 as well as coarse-2. Results are captured in the stack temperature at upstream and downstream, and the absolute relative errors are evaluated and summarized in Table 1. A compromise between accuracy and computation time was sought particularly when soliciting long unsteady solution. Therefore, a baseline mesh at an absolute temperature error values of 0.7% compared to the 1.5% and 10.7%, for coarse 1 and 2, respectively. A very strict residual of 10E-11 was targeted for all the considered levels.

Table 1. Mesh sensitivity results

Mesh level	Numb.of Cells	Up Temp (°C)	Down Temp (°C)	Temp Diff, (°C)	Rel. Err (%)
Fine	76,262	405.35	322.73	82.62	-----
Baseline	30,003	405.93	322.72	83.21	0.71
Coarse-1	21,293	406.58	322.70	83.88	1.52
Coarse-2	17,617	414.24	322.74	91.50	10.7

Table 2 summarizes the properties of the selected working fluids and it lists the theoretical and the obtained numerical values of the acoustic speeds. Accordingly, as the obtained numerical values are in agreement with the anticipated values, it provides further validity to the undertaking model.

Table 2. Calculated equivalent properties for different cases at the wavelength of sound $\lambda=30\text{cm}$

Case Study	C_p (J/kg.K)	C_v (J/kg.K)	γ Cp/Cv	Thermal Cond. (W/m.K)	Viscosity (Pa.s)	Molecular Weight (g)
W1 - He 100%	5193	3120	1.66	0.1520	1.99E-5	4.00
W2 - (25% He, 75% Air)	2053	1318	1.56	0.0562	1.84E-5	22.72
W3 - (50% He, 50% Air)	3099	1919	1.62	0.0881	1.90E-5	16.49
W4 - (70% He, 30% Air)	3937	2399	1.64	0.1137	1.92E-5	11.49
W5 - CO ₂ 100%	840.4	655.0	1.28	0.0145	1.4E-5	44.00
W6 - (25% CO ₂ , 75% Air)	964.9	702.3	1.37	0.0218	1.7E-5	32.77
W7 - (50% CO ₂ , 50% Air)	923.4	686.5	1.35	0.0194	1.6E-5	36.48
W8 - (70% CO ₂ , 30% Air)	890.2	673.9	1.32	0.0174	1.5E-5	39.49
W9- Air 100%	1006.4	718.0	1.40	0.0242	1.8E-5	28.97

3.2. Working Fluid Study

The working fluid sensitivity was conducted using the temperature gradient from 1,000 K to 300 K. This sensitivity was carried out initially for four compositions for each gas mixture, i.e. Helium – air and CO₂ - air. The first case (W1) was with using Helium gas as single working fluid, and the second (W2) was using the mixture ratio (25:75) of Helium with air gas. The third (W3) case was using the mixture ratio (50:50) of Helium with air gas, whereas the fourth case (W4) was using the mixture ratio (70:30) of Helium with air gas. The corresponding cases for the CO₂ – air mixture are denoted as W5, W6, W7 and W8. The W9, however represents the case of using air gas only.

Results for the pressure monitor placed at 14 cm downstream are analyzed. The results are compared with a single case of ‘Air only’ working fluid for better understanding. In cases W2, W3, W4, W5, W6, W7, W8, and W9 it was noticed that there is clear formation of a standing wave in the resonator. For W1 with the Helium gas, there is a bleak pressure fluctuation in first few time steps, which quickly dies out. Fig. 2 shows these results.

One can clearly notice that the onset of the standing wave is quickest for the Helium mixture, followed by ‘Air only’ cases then finally the CO₂ – air mixtures. To understand this behavior, it is important to study the equivalent properties which are shown in Table 2. In case of He –air mixture the thermal conductivity seems to increase as the share of air increases. It is a trivial fact that it is the thermal interaction between the thermal stack and the working fluid is what allows the development of a standing wave. With increase in conductivity the working fluids heats up faster, and thereby it initiates the pressure fluctuation much quicker. Comparing the compositions of He and CO₂ cases, it is evident that Helium mixtures have much higher thermal conductivity than CO₂ mixtures. This explains why the onset of the pressure wave is quicker for He mixtures compared to CO₂ mixtures. Even more evidence for this correlation can be found in the analysis of the wave for different CO₂ mixtures. In this case, with increasing air fraction the thermal conductivity decreases and the response is a clear delay in the pressure wave development. It must also be noticed that the c_p is also increasing in the He mixture cases, however it seems that the high temperature gradient prescribed at the stack provides sufficient energy to counter a delay in pressure wave onset. The viscosity variation is miniscule in these cases; therefore, it would not be appropriate to correlate the results with this property.

When any of the gases, i.e. He, CO₂ and air are individually considered as working fluids, it is seen that there is a pressure wave formation in the case of air and CO₂, but not in the case of He. Upon analysis of the properties, it appears that the molecular weight and the thermal conductivity, or rather, the tradeoff between these two properties is the controlling factor. In the case of He, the low molecular weight, resulting in less mass and added to that the high c_p seems to restrict the pressure wave development. Air, having a median molecular weight and median thermal conductivity that develops a pressure wave quicker than CO₂. Although CO₂ does show a standing

wave, the onset is delayed due to low thermal conductivity.

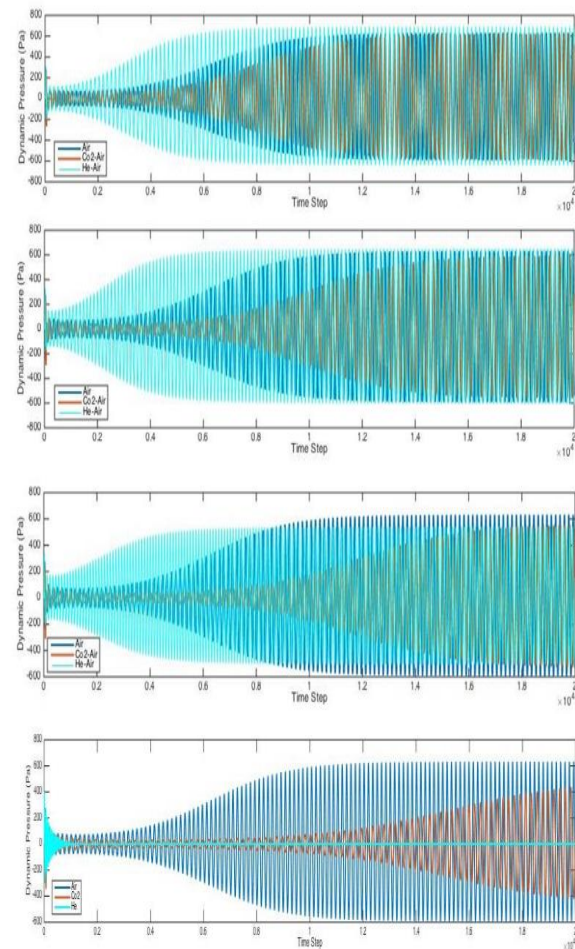


Figure 2. Static pressure wave development in the resonator for the Helium Gas cases (Top-Down: 25% Gas + 75% Air, 50% Gas + 50% Air, 70% Gas + 30% Air, Individual working fluids)

3.3. Frequency and Acoustic Speed Analysis

Fig. 3 shows the analysis of different frequencies obtained in the different cases. A particular but opposite trend is seen in cases of He and CO₂ mixtures. With increase in He in the system, the frequency increases, while increase in CO₂ reduces the frequency.

Peculiarly the molecular weight in the system decreases in the He mixtures, while it increases in the CO₂ mixtures. One expects that the speed of sound to be higher in denser mixtures and in turn reporting a higher frequency, but rather the case seems to be quite contrary. The explanation lies again in the thermal properties of gases. It is a common phenomenon that in hotter gases the speed of sound is higher compared to colder gases, although one expects the colder gases to be denser and by principle the speed of sound to be higher. Nevertheless, hotter gases have higher kinetic energy and thus there will be more potential for vibrations to occur. This leads to an increase in the speed of sound in the hotter gases. In this system the effect on frequency is likely a combined consequence of c_p , thermal conductivity and molecular weight. In He mixtures with increase in He the increasing c_p is balanced by the reducing mass while the thermal conductivity

increases, thus potentially causing higher temperatures and in turn higher frequencies. Whereas in CO₂ mixtures, the decreasing c_p is balanced with increasing molecular weight while the thermal conductivity decreases. This can potentially cause lower temperatures and thus lower frequencies.

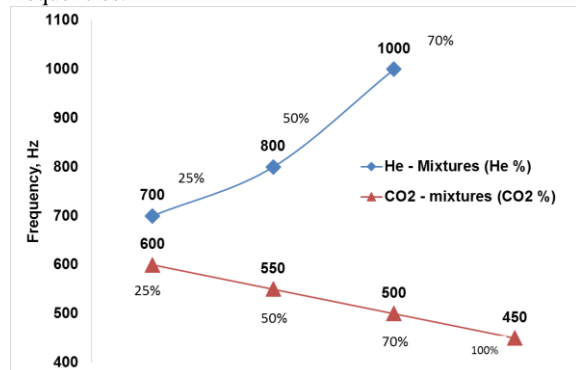


Figure 3. Analyzed frequencies for different working fluid cases

Further validation of this work is pertained to the evaluation and assessment of both thermal and viscous penetration lengths. These values are summarized in Table 3 for each of the successful runs. It is also in agreement with Swift recommendation. On one hand their ratio is near the value of the Prandtl number which close to unity for these near ideal gases. On the other hand, their values are only several folds of the distance between the stacks as indicated by Swift et al.

4. Conclusion

In this work numerical simulation of a Thermo-acoustic heat engine was carried out. The pressure wave in the resonator was analyzed for its time inception and the resulted frequency. The study aimed to understand the effect of working fluid in the thermo-acoustic engine and study the crucial properties affecting the pressure wave. Gas mixtures of He – air and CO₂ – air was assumed and the compositions were varied. The equivalent properties were prescribed in the system.

It is noticed that in He mixtures the onset of pressure wave is quicker than in only air or CO₂ mixtures. This was attributed to the He higher thermal conductivities. However, when only He was considered there was no pressure wave development. It was unlike the single gas of air or CO₂ cases. This was attributed to the low molecular weight of the He. Frequency in He mixtures rises as He composition is increased, while the contrary was observed in CO₂ mixtures. This is due to the collective consequence of the c_p , thermal conductivity and molecular weight. The

study shows how important the thermal properties of the working fluid are for the pressure wave. The variation in viscosity was miniscule, and therefore no conclusions were drawn to this respect. It must also be acknowledged that a perfectly mixed system is assumed whereas in real cases diffusion characteristics of gases may play a role.

Table 3. Evaluated properties corresponding to the 9 different cases

Case	Frequency	δk	δv	$\delta k / \delta v$
W1 - He 100 %	-	-	-	-
W2 - (25% He, 75% Air)	700	1.14E-4	9.32E-5	1.22
W3 - (50% He, 50% Air)	800	1.27E-4	1.03E-4	1.23
W4 - (70% He, 30% Air)	1000	1.37E-4	1.12E-4	1.22
W5 - CO ₂ 100%	450	7.85E-5	7.00E-5	1.12
W6 - (25% CO ₂ , 75% Air)	600	1.76E-4	7.95E-5	2.22
W7 - (50% CO ₂ , 50% Air)	550	1.84E-4	7.55E-5	2.44
W8 - (70% CO ₂ , 30% Air)	500	1.93E-4	7.37E-5	2.62
W9 - Air 100%	650	9.80E-5	8.46E-5	1.16

References

- [1] Guoyao Y, Dai W, Ercang L. CFD simulation of a 300 Hz thermoacoustic standing wave engine. *Cryogenics* 2010; vol. 50, pp. 615-622.
- [2] U. S. D. of. Energy Information, *Stirling Engine with Air Working Fluid*, 1985.
- [3] Ceperley P. Gain and efficiency of a short traveling wave heat engine. *J. Acoust. Soc. Am.* 1985 vol. 77, no. 3, pp. 1239-1244.
- [4] Swift, G. W., & Engines, S. (n.d.). Gregory W. Swift.
- [5] Nijeholt, J. A. L., Tijani, M. E. H., & Spoelstra, S. (2005). Simulation of a Traveling-Wave Thermoacoustic Engine Using Computational Fluid Dynamics. *J. Acoust. Soc. Am.* vol. 118, pp. 2265-2270.
- [6] Yazaki, T., Iwata, A., Maekawa, T., & Tominaga, A. (1998). Traveling Wave Thermoacoustic Engine in a Looped Tube. *Physical Review Letters*. vol. 81, pp. 3128 – 3131.
- [7] Biwa, T., Hasegawa, D., & Yazaki, T. (2010). Low Temperature Differential Thermoacoustic Stirling Engine. *Applied Physics Letters*. vol 97, pp. 1-3.
- [8] Backhaus, S., Tward, E., & Petach, M. (2004). Traveling Wave Thermoacoustic Generator. *Applied Physics Letters*. vol 85, pp. 1085-1087.
- [9] Russell, D. A., & Weibull, P. (2002). Tabletop Thermoacoustic Refrigerator for Demonstrations. *Am. J. Phys.* vol 70, no. 12, pp. 1231-1233.
- [10] Hussain, M. N., & Janajreh, I. (2017). Analysis of Pressure Wave Development in a Thermo-acoustic Engine and Sensitivity Study. *Energy Procedia*, 142, 1488-1495. <https://doi.org/10.1016/j.egypro.2017.12.597>.